Crystal Structures, Metal Activation, and DNA-Binding Properties of Two-Domain IdeR from *Mycobacterium tuberculosis*[†,‡]

Goragot Wisedchaisri,[§,||] C. James Chou,[§,⊥,#] Meiting Wu,[||] Claudia Roach,[||] Adrian E. Rice,[||,△] Randall K. Holmes,[○] Craig Beeson,[◇] and Wim G. J. Hol[*,||,□]

Department of Biochemistry and Biomolecular Structure Center, Department of Chemistry, and Howard Hughes Medical Institute, University of Washington, Seattle, Washington 98195, Department of Microbiology, University of Colorado School of Medicine, Aurora, Colorado 80045, and Department of Pharmaceutical Sciences, Medical University of South Carolina, Charleston, South Carolina 29425

Received May 17, 2006; Revised Manuscript Received October 20, 2006

ABSTRACT: The iron-dependent regulator IdeR is a key transcriptional regulator of iron uptake in *Mycobacterium tuberculosis.* In order to increase our insight into the role of the SH3-like third domain of this essential regulator, the metal-binding and DNA-binding properties of two-domain IdeR (2D-IdeR) whose SH3-like domain has been truncated were characterized. The equilibrium dissociation constants for Co^{2+} and Ni^{2+} activation of 2D-IdeR for binding to the *fxbA* operator and the DNA-binding affinities of 2D-IdeR in the presence of excess metal ions were estimated using fluorescence spectroscopy. 2D-IdeR binds to *fxbA* operator DNA with similar affinity as full-length IdeR in the presence of excess metal ion. However, the Ni^{2+} concentrations required to activate 2D-IdeR for DNA binding appear to be smaller than that for full-length IdeR while the concentration of Co^{2+} required for activation remains the same. We have determined the crystal structures of Ni^{2+}-activated 2D-IdeR at 1.96 Å resolution and its double dimer complex with the *mbtA-mbtB* operator DNA in two crystal forms at 2.4 Å and 2.6 Å, the highest resolutions for DNA complexes for any structures of iron-dependent regulator family members so far. The 2D-IdeR−DNA complex structures confirm the specificity of Ser37 and Pro39 for thymine bases and suggest preferential contacts of Gln43 to cytosine bases of the DNA. In addition, our 2D-IdeR structures reveal a remarkable property of the TEV cleavage sequence remaining after removal of the C-terminal His_6. This C-terminal tail promotes crystal contacts by forming a β-sheet with the corresponding tail of neighboring subunits in two unrelated structures of 2D-IdeR, one with and one without DNA. The contact-promoting properties of this C-terminal TEV cleavage sequence may be beneficial for crystallizing other proteins.

Iron is an essential element for the growth of most organisms. The concentration of free iron in human tissues and body fluids is far below the normal growth requirements for pathogens due to the chelation by transferrin, lactoferrin, heme, and ferritin which (i) protect human cells from oxidative damages caused by free iron and (ii) provide a protective low-iron barrier against infectious agents (*1*). To overcome the low availability of iron, *Mycobacterium tuberculosis*, one of the world's major pathogens that is responsible for 2 million deaths per year worldwide from tuberculosis (*2*), has developed an elaborate iron uptake system, which at the same time is tightly regulated to prevent oxidative damage to the microorganism itself from excess iron (*1*).

The iron-dependent regulator IdeR is the key regulator of iron uptake in mycobacteria (*3*−*5*). IdeR has been shown to be essential for the growth of *M. tuberculosis* as a disruption of the *ideR* gene in the absence of a second functional copy in the bacteria is lethal (*6*). IdeR regulates about 40 *M. tuberculosis* genes involved in iron uptake and metabolism by binding to operator regions of these genes and usually repressing transcription, although the transcription of a few genes is enhanced (*5*). Many of these genes are involved in the synthesis, export, and import of siderophores, small molecule chelating agents with high affinity for iron, such as mycobactin and its derivatives (*7*, *8*). A ten-gene cluster, designated *mbtA* to *mbtJ*, spanning 24 kilobases of the *M. tuberculosis* genome, encodes gene products that are enzymes in the mycobactin biosynthesis pathway (*9*). Two so-called

[†] This work was supported by NIH Grants CA65656 to W.G.J.H. and AI14107 to R.K.H.

[‡] The atomic coordinates and structure factors of 2D-IdeR and two 2D-IdeR−DNA complexes, crystal forms I and II, have been deposited with the RCSB Protein Data Bank with the accession numbers 2ISY, 2ISZ, and 2IT0, respectively.

* To whom correspondence should be addressed. E-mail: wghol@u.washington.edu. Tel: (206) 685-7044. Fax: (206) 685-7002.

[§] G.W. and C.J.C. contributed equally to the work.

[||] Department of Biochemistry and Biomolecular Structure Center, University of Washington.

[⊥] Department of Chemistry, University of Washington.

[#] Present address: Department of Molecular Biology, Scripps Research Institute, 10550 North Torrey Pines Road, MB-27, La Jolla, CA 92037.

[△] Present address: Department of Biochemistry and Molecular Biophysics, California Institute of Technology, M/C 114-96, Pasadena, CA 91125.

[○] University of Colorado School of Medicine.

[◇] Medical University of South Carolina.

[□] Howard Hughes Medical Institute, University of Washington.

10.1021/bi0609826 CCC: $37.00 © 2007 American Chemical Society
Published on Web 12/19/2006

"iron boxes", the *mbtA-mbtB* and *mbtI* operators, were identified in this gene cluster, and IdeR was shown to bind to both operators in vitro (*5*). The binding of activated IdeR to the *mbtA-mbtB* and *mbtI* operators, which occurs when iron levels in the cell are high, represses the transcription of *mbtA-J* genes, thereby limiting the synthesis of mycobactin and, consequently, iron uptake into the cell. In *Mycobacterium smegmatis*, exochelin is another key siderophore involved in iron uptake (*10*). A putative enzyme formyl transferase involved in exochelin biosynthesis is encoded by the *fxbA* gene (*10*, *11*). IdeR was shown to bind to the operator region of the *fxbA* gene in *M. smegmatis* under high Fe^{2+} concentrations and to repress expression of the *fxbA* gene (*11*).

M. tuberculosis IdeR contains three domains and two metal-binding sites (*12*). The N-terminal 74 residues belong to domain 1, which is homologous to the winged helix−turn−helix DNA-binding domain. Domain 2 includes residues 75−140, provides most metal coordinating ligands, functions as a dimerization domain, and is connected to domain 3 by a flexible linker. Domain 3 is an SH3[1]-like domain (*12*, *13*) consisting of residues 151−230. Apo-IdeR is very flexible and has a preferential monomeric form which is in equilibrium with a dimeric form (*14*). Dimerization occurs when iron-binding site 1 is occupied in both monomers at a low iron concentration, and activation of DNA-binding activity occurs when iron-binding sites 1 and 2 are occupied in both monomers at a higher iron concentration (*14*). In addition to activation by Fe^{2+}, IdeR can be activated by Co^{2+}, Ni^{2+}, Mn^{2+}, Cd^{2+}, and Zn^{2+} in vitro (*15*). A conformational change of the hinge region at residue 74 was observed in metal-activated IdeR structures and was proposed to be a basis for bringing the DNA-binding domains of two subunits in a dimer closer together and increasing the DNA-binding affinity (*12*, *16*). The SH3-like domain repositions itself to coordinate the metal at site 1 using residues Glu172 and Gln175 and has been suggested to play an important structural role in stabilizing the active conformation of IdeR (*12*). Mutagenesis studies have shown that the SH3-like domain is important for the activation regulation in DtxR, an IdeR homologue from *Corynebacterium diphtheriae* (*17*, *18*). NMR studies have suggested that the SH3-like domain of DtxR stabilizes a monomer form of the regulator by binding to a proline-rich region within the dimerization domain (*19*, *20*). It is possible that the SH3-like domain regulates IdeR activities through interactions with multiple regions within the regulator in the absence of metal ion.

In this study, we investigated the structure and function of a two-domain variant of IdeR with a deletion of the SH3-like third domain for comparison with previous data on full-length IdeR (*14*, *21*). The metal-dependent affinity of 2D-IdeR for the *fxbA* operator was characterized using a fluorescence anisotropy assay. Additionally, crystal structures of Ni^{2+}-activated 2D-IdeR were determined to 1.96 Å in the absence of DNA duplex and to 2.4 and 2.6 Å for the complex with *mbtA-mbtB* operator DNA in two crystal forms. Our results indicate the following:

(i) 2D-IdeR is already dimerized in the absence of divalent metal ion, suggesting a key role for the SH3-like domain to stabilize the monomer and prevent dimerization in the absence of metal ion.

(ii) The apparent affinities for divalent metal ions at site 1 are not sensitive to loss of metal ligands provided by the SH3-like domain.

(iii) The high-resolution structures of the 2D-IdeR−DNA complex provide details of DNA base-specific interactions of Ser37 and Pro39 for thymine as observed in the lower resolution structures of IdeR−DNA and DtxR−DNA complexes previously determined (*21*−*24*).

(iv) The high-resolution structures indicate a distinctive role of Gln43 for its preferential hydrogen bonding to the cytosine base of the DNA.

(v) The artificial C-terminal tail of 2D-IdeR introduced from the TEV cleavage sequence promotes crystal contacts by forming a β-sheet with neighboring subunits.

EXPERIMENTAL PROCEDURES

Construction of the Expression Plasmid. The DNA fragment of the 2D-IdeR gene encoding amino acid residues 1−140 was amplified by PCR from a full-length IdeR plasmid DNA (*15*) using oligonucleotide primers *ider140*-S1 (5′-GCACATATGAACGAGTTGGTTGATACC-3′) and *ider140*-A1 (5′-ATAGCTAGCCACGCCAAGTTCCACCAG-3′) and *PfuTurbo* DNA polymerase (Stratagene). The PCR product was digested and ligated with T4 DNA ligase using *Nde*I and *Nhe*I restriction sites into pAER36, an in-house vector derived from pET-29b(+) vector (Novagen) of which an *Nhe*I restriction site, a TEV protease cleavage sequence, and a His_6 tag were cloned into the *Bam*HI site. The plasmid was introduced into *Escherichia coli* BL21(DE3) (Novagen). 2D-IdeR expressed by this plasmid includes native residues 1−140 plus a TEV-cleavable His_6 tag ASENLYFQ∧GGGHHHHHH sequence at the C-terminus, where ∧ indicates the TEV cleavage position.

Protein Expression and Purification. The *E. coli* cells containing the expression plasmid were grown in LB media at 37 °C until the OD_{600} was 0.6. The temperature was then reduced to 27 °C, and the cells were induced for expression with 0.5 mM IPTG for 4 h and subsequently harvested by centrifugation at 5000 rpm for 15 min at 4 °C. The cell pellets were lysed using a French press in a lysis buffer containing 20 mM Tris-HCl, pH 8.0, 300 mM NaCl, 5 mM β-mercaptoethanol, and 1 mM PMSF, and the lysate was subsequently centrifuged at 13000 rpm for 20 min at 4 °C. The supernatant was incubated with Ni-NTA resin at 4 °C for 1 h. The mixture was poured into a plastic column and washed with a buffer containing 20 mM Tris-HCl, pH 8.0, 300 mM NaCl, 5 mM β-mercaptoethanol, and 20 mM imidazole for 10 column volumes, and 2D-IdeR was eluted with the same buffer containing 250 mM imidazole for 5 column volumes. The eluted fractions were combined, and TEV protease was added to 2D-IdeR to remove the His_6 tag with a protein:TEV protease ratio of 50:1 and dialyzed to a buffer containing 20 mM Tris-HCl, 300 mM NaCl, and 5 mM β-mercaptoethanol at 4 °C overnight. The TEV protease was the His_6-tagged version that can be removed from the cleaved 2D-IdeR when it is subsequently passed over Ni-NTA resin. The cleaved 2D-IdeR contains native residues 1−140 plus eight C-terminal residues with the ASENLYFQ sequence. The cleaved protein was then incubated with Ni-NTA resin,

[1] Abbreviations: 2D-IdeR, two-domain iron-dependent regulator; SH3, src-homology 3; TEV, tobacco etch virus.

and the flow-through fraction was collected. The protein was subsequently concentrated and purified using a Superdex 75 HiLoad 16/60 size-exclusion column equilibrated with a buffer containing 20 mM Tris-HCl, pH 8.0, 300 mM NaCl, 1 mM EDTA, and 1 mM TCEP. The peak fractions were combined and dialyzed against buffer containing 20 mM Tris-HCl, pH 7.0, 50 mM NaCl, 1 mM EDTA, and 1 mM TCEP. The purified 2D-IdeR aggregated over time, and the soluble fraction lost its activity after 1 week. Therefore, the protein was flash frozen according to the protocol of Deng et al. (*25*) and stored at −80 °C for fluorescence anisotropy assays.

Fluorescence Anisotropy Assay. Fluorescein-labeled *fxbA* operator DNA for the fluorescence anisotropy assay was prepared as described previously (*14*). Fluorescence anisotropy measurements were performed in a SPEX Fluorolog 1681 0.22 m spectrometer (Jobin YVON-SPEX, Edison, NJ) with polarizers placed in L-format. The measurements were taken at an excitation wavelength of 490 nm and emission wavelength of 525 nm. Frozen 2D-IdeR pellets were thawed before use according to the protocol of Deng et al. (*25*). Divalent metal dependent DNA-binding affinities were determined by titrating Ni^{2+} and Co^{2+} in 1 and 5 μM increments, respectively, into a buffer containing 2 μM 2D-IdeR, 20 nM *fxbA* operator duplex, 5 mM Mg^{2+}, 50 mM NaCl, 20 mM Tris-HCl, 60 mg/mL acetylated BSA, and 10 mg/mL poly(dI-dC) nucleotides at pH 7.0. For the IdeR−*fxbA* operator affinity determination, 2D-IdeR was titrated in 0.025 μM increments into a buffer containing 20 nM *fxbA* operator duplex, 5 mM Mg^{2+}, 50 mM NaCl, 20 mM Tris-HCl, 60 mg/mL acetylated BSA, and 10 mg/mL poly(dI-dC) nucleotides at pH 7.0, with or without 0.2 mM Ni^{2+}. All solutions were treated with Chelex 100 and sterile filtered before use. Steady-state fluorescence anisotropy, *r*, was calculated as described previously (*14*). The *r*-value is normalized to the maximum among the Ni^{2+} and Co^{2+} experiments.

The DNA-binding activity of 2D-IdeR was evaluated by measuring changes in the fluorescence anisotropy value of a 5′-end-labeled *fxbA* operator. In the presence of excess divalent metal ions, the association of 2D-IdeR with the *fxbA* operator was expressed as the binding of two dimers to form a tetrameric protein−DNA complex. The detailed calculation method was described previously (*14*).

Dynamic Light Scattering. The hydrodynamic radius and estimated IdeR molecular weight were determined using Protein Solutions DynaPro molecular sizing instruments (Protein Solutions Ltd., Bucks, England) as described before (*14*). Measurements were taken using 1 mg/mL 2D-IdeR in a buffer solution containing 20 mM Tris-HCl, pH 7.0, 5 mM Mg^{2+}, and 50 mM NaCl at 20 °C.

Crystallization. Fresh 2D-IdeR protein after purification was used immediately for crystallization to obtain good quality crystals. Sitting-drop vapor diffusion at room temperature was used for all crystallization experiments. Crystals of 2D-IdeR were obtained by mixing 2 μL of 0.24 mM protein solution with 2 μL of 4 mM $NiCl_2$ and 2 μL of precipitant solution containing 0.6 M sodium/potassium phosphate, pH 8.2. The crystals were transferred to a cryoprotectant solution containing 0.6 M sodium/potassium phosphate, pH 8.2, 35% glycerol, 4 mM $NiCl_2$, and 10 mM cyclic peptide (see below) and subsequently flash frozen by immersion into liquid nitrogen.

The 2D-IdeR−DNA complex was prepared by mixing 2D-IdeR protein with a 33mer oligonucleotide duplex containing the *mbtA-mbtB* operator sequence as described previously (*21*) in a 3:1 protein:DNA molar ratio. The 2D-IdeR−*mbtA-mbtB* operator complex in crystal form I was obtained by mixing 0.7 μL of complex solution containing 0.24 mM 2D-IdeR (4 mg/mL), 0.08 mM DNA, and 2 mM $NiCl_2$ with 0.7 μL of precipitant solution containing 28% PEG 3350, 0.2 M ammonium acetate, and 0.1 M Bis-Tris, pH 7.5. The crystals were transferred to a cryoprotectant solution containing 30% PEG 3350, 0.2 M ammonium acetate, 0.1 M Bis-Tris, pH 7.5, 15% glycerol, and 2 mM $NiCl_2$ and subsequently flash frozen by immersion into liquid nitrogen. The above solutions also contained 5 mM cyclic peptide, ELh-CQAKSEKhC (where hC is homocystine), which was designed to bind to the IdeR−DNA complex. However, no electron density from the peptide was observed, and its inclusion in the buffers did not affect the crystallization.

The 2D-IdeR−*mbtA-mbtB* operator complex in crystal form II was obtained by mixing 2 μL of complex solution containing 0.24 mM 2D-IdeR (4 mg/mL), 0.08 mM DNA, and 2 mM $NiCl_2$ with 2 μL of precipitant solution containing 26% PEG 4000, 0.2 M sodium acetate, 0.1 M Tris-HCl, pH 8.5, and 5% glycerol. The crystals were transferred to a cryoprotectant solution containing 30% PEG 4000, 0.2 M sodium acetate, 0.1 M Tris-HCl, pH 8.5, 20% glycerol, and 1 mM $NiCl_2$ and subsequently flash frozen by immersion into liquid nitrogen. The cyclic peptide was not used in this experiment.

Data Collection and Structure Determination. Diffraction data were collected at ∼1 Å wavelength at the Advanced Photon Source (APS) beamline 19-ID for the uncomplexed 2D-IdeR and at the Advanced Light Source (ALS) beamline 8.2.2 for the 2D-IdeR−*mbtA-mbtB* operator complexes. The data for the uncomplexed 2D-IdeR and 2D-IdeR−*mbtA-mbtB* complex in crystal form I were indexed, integrated, and scaled with HKL2000 (*26*) in space group *P*1. The structure of 2D-IdeR was solved by molecular replacement using the program Molrep (*27*) with a model derived from the full-length IdeR monomer (*12*) truncated to residues 1−140. The asymmetric unit contains two 2D-IdeR subunits forming a dimer.

The structure of the 2D-IdeR−*mbtA-mbtB* operator complex in crystal form I (space group *P*1) was solved by molecular replacement using the program Molrep (*27*) with a model of the full-length IdeR−*mbtA-mbtB* operator complex (*21*) truncated to residues 1−140 for all four protein subunits (A−D) and nucleotide residues 4−26 and 7−29 for DNA chains E and F, respectively. The asymmetric unit contains four 2D-IdeR subunits and two oligonucleotide strands forming a double dimer 2D-IdeR−double-stranded DNA complex. Several cycles of NCS restrained refinement and manual model correction were carried out using the program Refmac (*28*) and Xtalview (*29*), respectively. Subsequently, automated water placement by the program Coot (*30*) was used to add water molecules. Refinement was completed after iterative cycles of model correction using Coot (*30*) and refinement using Refmac (*28*) without NCS restraints. Although the cyclic decapeptide was present in the cryoprotectant solutions of two of the above mentioned crystal forms, no electron density representing the peptide was observed.

The diffraction data for the 2D-IdeR−DNA complex in crystal form II were indexed, integrated, and scaled with the automated program Elves (*31*) using Mosflm (*32*) and Scala (*33*) in space group *P*1. The structure of the 2D-IdeR−*mbtA*-*mbt*B operator complex in crystal form II was solved by molecular replacement using the program Molrep (*27*) with a model of the 2D-IdeR−*mbtA*-*mbt*B operator complex from the structure of crystal form I. The asymmetric unit contains four 2D-IdeR subunits and two oligonucleotide strands forming a double dimer 2D-IdeR−double-stranded DNA complex. Refinement was completed after iterative cycles of model building and water placement using Coot (*30*) and refinement using Refmac (*28*).

RESULTS

Metal-Dependent DNA-Binding Assays. By taking advantage of Trp104 located at the dimerization interface of IdeR, we have previously used quenching of the intrinsic IdeR tryptophan fluorescence to monitor the metal ion dependent dimerization of full-length IdeR monomers (*14*). In the current work, upon addition of divalent metal ions to 2D-IdeR, quenching of the intrinsic fluorescence was not observed (not shown), even though the tryptophan residues of IdeR are not anywhere near the region truncated in 2D-IdeR. It has been shown that full-length DtxR and IdeR proteins are monomeric at low concentrations in the absence of divalent metal ions. Protein dimerization is observed upon increase in protein concentration (>50 μM) or upon addition of divalent metal ion (*14*). The reported DLS measured Stokes radii $R_h = 2.3$ nm and $R_h = 2.9$ nm for native IdeR protein (25 kDa) solution at 1 mg/mL concentration in the absence and presence, respectively, of divalent metal ion correspond to estimated masses of 29 and 54 kDa (*14*). In contrast, the autocorrelation function solutions for DLS measurements of 2D-IdeR protein (17 kDa) solution at the same concentration both with and without divalent metal ions gave an average Stokes radius of $R_h = 2.8$ nm, which corresponds to an estimated mass of 39 kDa indicating that 2D-IdeR forms a dimer in the absence of divalent metal ions (Figure S1). This suggests that 2D-IdeR is already a dimer in the absence of divalent metal ions. Therefore, from both the intrinsic Trp fluorescence and the dynamic light scattering studies, it appears that IdeR without its SH3-like domain the initial dimerization step does not require metal ion.

The Ni^{2+} and Co^{2+} dependence for 2D-IdeR binding to the *fxbA* operator was determined using the previously established fluorescence anisotropy assay (*14*). The K_d for 2D-IdeR activation by Co^{2+} is 25 μM (Figure 1a and Table S1), the same value as that determined previously for full-length IdeR (*14*). Interestingly, the K_d for activation of 2D-IdeR by Ni^{2+} decreased to 4 μM (Figure 1a and Table S1) from the value of approximately 13 μM determined previously for activation of full-length IdeR (*14*). Addition of the apo-2D-IdeR to fluorescein-labeled *fxbA* in the absence of metals did not change the *fxbA* fluorescence anisotropy, which demonstrates that the dimer does not bind to *fxbA* without metals.

The binding of 2D-IdeR to the *fxbA* operator duplex in the presence of excess divalent metal ion was also measured using fluorescence anisotropy methods as described previously (*14*). The DNA-binding affinity appeared to be ~0.17 μM for 2D-IdeR (Figure 1b), which is similar to the value previously reported for full-length IdeR (0.14 μM) (*14*). The result confirms that our 2D-IdeR variant is active and binds to operator DNA without a significant change in the binding affinity. This demonstrates that the SH3-like domain is not essential for DNA binding in vitro.

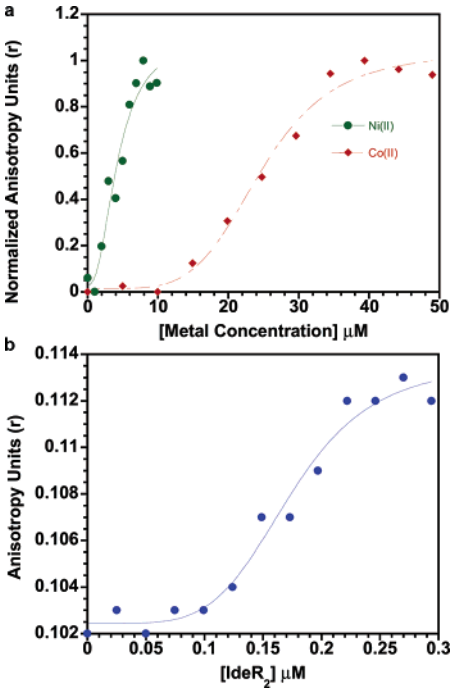

FIGURE 1: 2D-IdeR binding to the *fxbA* operator monitored by fluorescence anisotropy. (a) Metal-dependent titration of 2D-IdeR-*fxbA* operator binding. (b) 2D-IdeR binding to the *fxbA* operator duplex in an excess of metal ion. The 2D-IdeR concentration is corrected with the dilution factor. The K_d for 2D-IdeR binding is 0.17 ± 0.01 μM.

Crystal Structure of 2D-IdeR. A crystal structure of Ni^{2+}-activated 2D-IdeR has been determined at 1.96 Å resolution. The structure was refined to an R_{work} of 17.6% and R_{free} of 21.1% with good geometry (Table 1). The structure reveals in the asymmetric unit two subunits of 2D-IdeR forming a dimer with two Ni^{2+} ions binding to each protein molecule and one phosphate ion coordinating Ni^{2+} at metal-binding site 1 of each subunit (Figure 2a). The model includes residues 2−140 plus the additional C-terminal ASENLYFQ residues remaining from the N-terminal part of the TEV cleavage sequence after proteolysis with TEV protease. (The TEV cleavage sequence was incorporated into the C-terminal part of the protein construct to allow removal of the C-terminal His_6 tag after protein purification.) These C-terminal residues protrude into the solvent without making intramolecular interactions with the protein core. The electron density is excellent in most regions of the protein except for a loop between the "winged" β-strands ($\beta1-\beta2$) in the DNA-binding domain, reflecting flexibility in this region. The two subunits per dimer are very similar to each other with an rms deviation of 0.4 Å for the 147 C^α atoms from residues 2 to 148.

The Metal-Binding Sites. Each 2D-IdeR molecule contains two metal-binding sites (Table S2). The two sites appear to be fully occupied as shown by the height of the peaks in the $F_o - F_c$ difference electron density maps ($9\sigma-10.5\sigma$) calculated with the initial phases when omitting the metals.

Table 1: Data Collection and Refinement Statistics for Crystal Structures of 2D-IdeR

	2D-IdeR	2D-IdeR−DNA complex (crystal form I)	2D-IdeR−DNA complex (crystal form II)
data collection			
space group	*P*1	*P*1	*P*1
unit cell dimensions			
a, *b*, *c* (Å)	41.9, 44.7, 49.6	53.8, 69.7, 76.5	54.0, 70.4, 79.6
α, *β*, *γ* (deg)	110.2, 96.6, 108.3	106.6, 104.8, 99.7	108.9, 103.1, 94.8
resolution range[a] (Å)	50−1.95 (2.02−1.95)	50−2.4 (2.49−2.40)	50−2.6 (2.73−2.60)
total no. of reflections	36720	65232	59087
unique reflections	20610	34892	31514
$I/\sigma(I)$[a]	11.1 (3.7)	9.7 (2.0)	7.1 (1.9)
completeness[a] (%)	91.8 (58.1)	90.4 (60.7)	96.3 (95.9)
R_{merge}[a,b] (%)	6.0 (17.3)	7.5 (29.6)	12.6 (34.8)
refinement			
resolution range (Å)	50−1.96	50−2.4	50−2.6
no. of reflections used (working/free)	19548/1058	33135/1754	29912/1595
R_{work} (%)	17.6	19.9	22.6
R_{free} (%)	21.1	23.9	27.3
no. of protein residues	2−148 (A and B)	1−140 (A−D)	3−147 (A, B), 3−139 (C, D)
no. of water molecules	148	142	32
average *B*-factor of all atoms (Å^2)	28.6	40.3	25.5
rmsd from ideal geometry			
bond length (Å)	0.011	0.007	0.007
bond angle (deg)	1.28	1.13	1.19

[a] Values in parentheses refer to the outer shell reflections. [b] $R_{merge} = \Sigma|I - \langle I\rangle|/\Sigma\langle I\rangle$.

The *B*-factors of the metals (∼20 Å^2) are comparable to the *B*-factors observed for nearby side chains.

Ni^{2+} at metal-binding site 1 in each subunit is surrounded by protein and nonprotein ligands. Residues His79 ($N^{\epsilon 2}$), Glu83 ($O^{\epsilon 2}$), and His98 ($N^{\delta 1}$) provide three ligands (Figure 2b). The fourth ligand was the strongest peak (11.5σ−12σ) in the $F_o - F_c$ difference electron density map after the metal cations have been placed. This peak has a tetrahedral shape and appears to be a phosphate ion which contributes one of its oxygen atoms to the metal (Table S2). The phosphate ion in each subunit makes direct interactions with the His79 $N^{\epsilon 2}$, Arg80 N^{ϵ} and $N^{\eta 2}$, Gln83 $O^{\epsilon 1}$, Ser126 O^{γ}, and Asn130 $N^{\delta 2}$ atoms of the protein using its oxygen atoms with distances ranging between 2.6 and 3.2 Å. Two additional water molecules complete the coordination of the metal ion. There are six metal ligands in total at metal-binding site 1, forming a distorted octahedral geometry.

The cation at metal-binding site 2 is coordinated by six ligands, also resulting in a distorted octahedral geometry (Figure 2c). Four atoms are provided by the protein side chains of Met10 (S^{δ}), oxidized Cys102 (O^{δ}) (modeled as *S*-hydroxycysteine), Glu105 ($O^{\epsilon 1}$), and His106 ($N^{\delta 1}$). The other two ligand atoms are the main chain oxygen of Cys102 and a water oxygen linked to the carbonyl oxygen of Leu4 (Table S2).

The C-Terminal Tail. The C-terminal tail of 2D-IdeR (141-ASENLYFQ-148), remaining after proteolysis by TEV protease, forms an antiparallel *β*-sheet with the C-terminal tail of a neighboring molecule (Figure 3). The *β*-strand is seen in both subunits in the dimer and provides crystal contacts. To the best of our knowledge, this is the first time a protease cleavage sequence has been observed to form a crystal contact *β*-sheet.

Comparison with Full-Length IdeR. The 1.96 Å structure of the Ni^{2+}-activated 2D-IdeR dimer is very similar to the dimer formed by the first two domains in the previously determined 2.0 Å structure of Co^{2+}-activated full-length IdeR by Feese et al. (*12*). Superposition of 139 C^{α} atoms from residues 2−140 of the 2D-IdeR monomer structure onto those of the full-length structure yielded rms deviations of 0.4−0.6 Å, while superposition of the dimer results in an rms deviation of 0.6 Å.

At metal-binding site 1, oxygen atoms from two water molecules in the 2D-IdeR structure replace Glu172 $O^{\epsilon 1}$ (within 0.8 Å) and Gln175 $O^{\epsilon 1}$ (within 0.4 Å) atoms of the full-length structure (*12*). The phosphate oxygen atom coordinating metal site 1 has not been observed before and is not equivalent to any ligand atoms in the full-length structure of Feese et al. (*12*). It is interesting to note that in the Zn^{2+}-activated full-length IdeR structure of Pohl et al. (*16*) the SH3-like domain is invisible and a sulfate ion coordinates the metal site 1 with one of its oxygen atoms near the position of Glu172 $O^{\epsilon 1}$. However, the phosphate ion in the current 2D-IdeR structure is in a different position from the sulfate ion in the structure of Pohl et al. (*16*): the S and the P positions differ by 3.1 Å. The phosphate ion provides an extra coordination to the metal in addition to three ligands from the protein side chain and two water molecules. The additional coordination results in octahedral geometry at this binding site instead of the trigonal-bipyramidal geometry observed in the full-length structure of Feese et al. (*12*). Given the high phosphate concentration of 0.5 M in our crystallization buffer and the low physiological concentration of ∼10 mM, it is unlikely that this phosphate binding site is of physiological relevance.

The octahedral geometry of the metal-binding site 2 is similar to those from the full-length IdeR structures of Feese et al. (*12*) and Pohl et al. (*16*) except that Cys102 of 2D-IdeR is modeled in as an *S*-hydroxycysteine in two conformations due to oxidization of its S^{γ} atom. There is no significant structural change of the metal-activated conformation for the first two domains in the absence of the third domain.

Crystal Structures of the 2D-IdeR−DNA Complex. Two crystal structures of 2D-IdeR in complex with Ni^{2+} and the

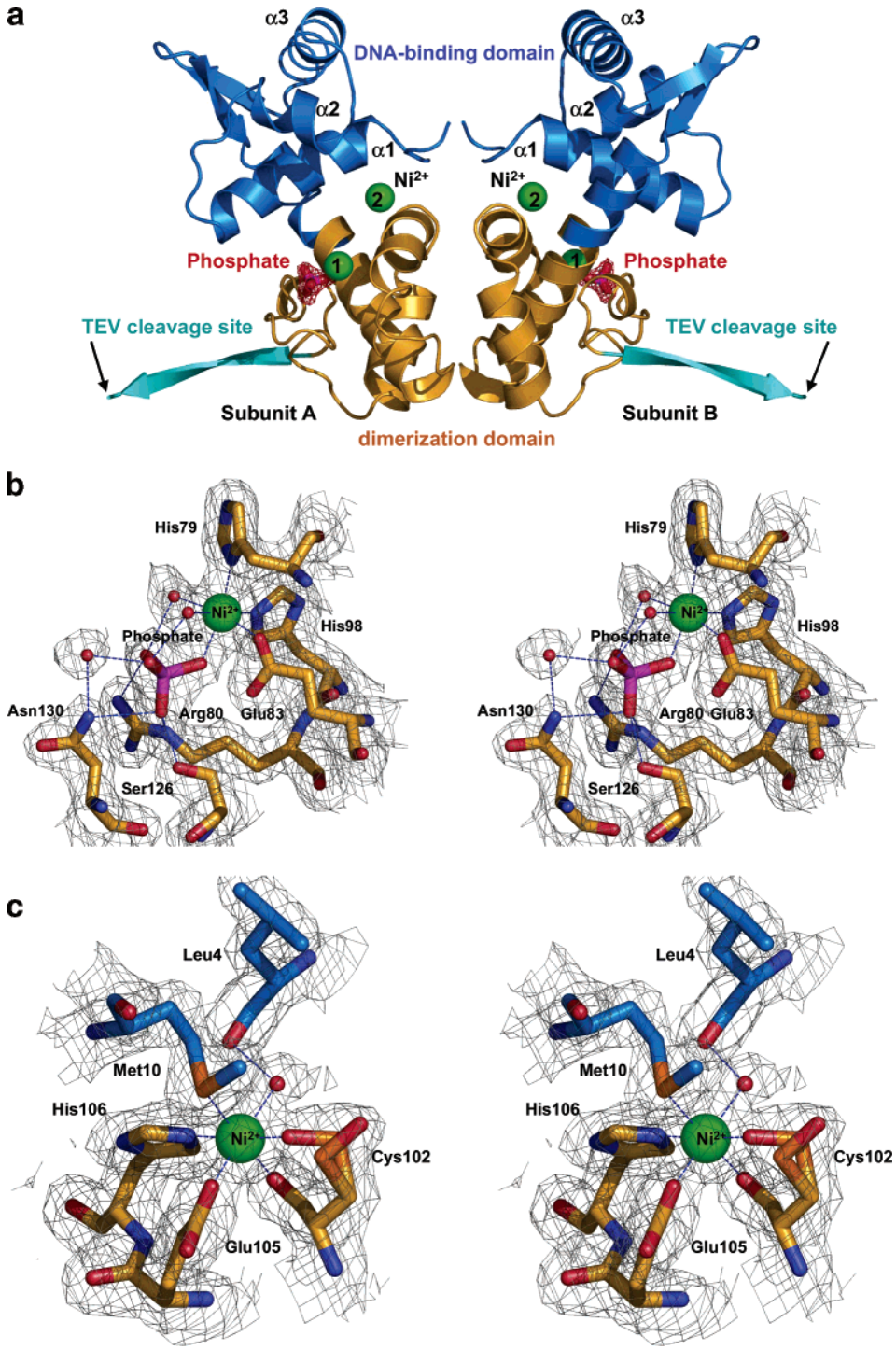

FIGURE 2: Crystal structure of Ni^{2+}-activated 2D-IdeR. (a) Crystal structure of the 2D-IdeR dimer viewed perpendicular to the 2-fold. Each 2D-IdeR subunit contains two metal-binding sites with one phosphate ion coordinating metal ion in binding site 1. The N-terminal DNA-binding domain is shown in blue, the dimerization domain in orange, and the C-terminal tail in cyan. Ni^{2+} ions are shown as green spheres. Phosphate ions are shown as stick models colored magenta for phosphorus and red for oxygen. The σ_A-weighted $F_o - F_c$ electron density at the 4.0σ contour level is shown in red around the phosphates. (b) Stereoview of metal-binding site 1 with the σ_A-weighted $2F_o - F_c$ electron density at the 1.0σ contour level. Three side chains of residues His79, Glu83, and His98, two water molecules, and a phosphate oxygen atom coordinate the metal to form an octahedral metal−ligand geometry. Phosphate ions also form hydrogen bonds to side chains of His79, Arg80, Gln83, Ser126, and Asn130. (c) Stereoview of metal-binding site 2 with the σ_A-weighted $2F_o - F_c$ electron density at the 1.0σ contour level. Side chains of Met10 from the DNA-binding domain, Cys102, Glu105, and His106 from the dimerization domain, the main chain carbonyl oxygen of Cys102, and a water molecule (bridging to the main chain carbonyl oxygen of Leu4) coordinate the metal to generate an octahedral metal−ligand geometry. Cys102 is modeled as *S*-hydroxycysteine in two conformations reflecting the oxidization state of this residue.

mbtA-mbtB operator DNA were determined at 2.4 Å (crystal form I) and 2.6 Å (crystal form II) (Table 1). Due to similarity between the two structures (rms deviations of 0.4 Å for 468 C^{α} atoms of core residues 4−120 from four protein subunits and 0.8 Å for all protein and DNA atoms), only the highest resolution structure (crystal form I) is described here. However, key differences of the two crystal forms are noted.

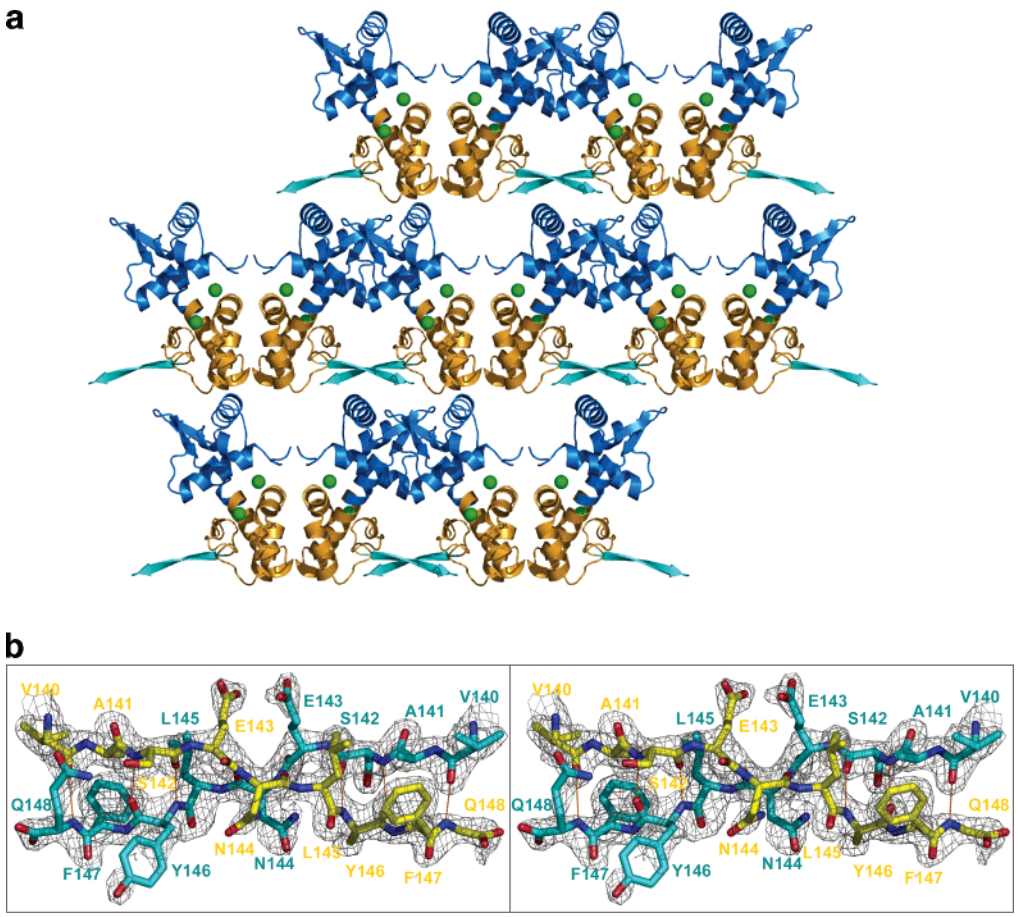

FIGURE 3: Crystal packing of 2D-IdeR. (a) The C-terminal tail containing the TEV cleavage sequence (ASENLYFQ) forms a β-sheet to provide crystal contacts to neighboring molecules. (b) Stereoview of the C-terminal tail with the σ_A-weighted $2F_o - F_c$ electron density at the 1.0σ contour level. The C-terminal tail is shown in stick model in cyan for subunit A and yellow for subunit B′, which is symmetry-related to subunit B.

The asymmetric unit of both crystal forms contains four 2D-IdeR subunits, one double-stranded oligonucleotide duplex, and twelve Ni^{2+} ions (Figure 4a). Each protein subunit contains three Ni^{2+} ions of which two are essentially at the metal-binding sites 1 and 2 (Table S2). A third Ni^{2+} is found near the side chain of His61 as judged by its 10.6σ−13.9σ peak in the σ_A-weighted $F_o - F_c$ map. The third metal-binding site is different from that found in the SH3-like third domain of the full-length IdeR and DNA complex structures (*12*, *21*). This metal-binding site has not been observed in previous IdeR structures (*12*, *16*, *21*) and may not have physiological significance.

2D-IdeR−DNA Interactions. Due to their higher resolution, the structures of the 2D-IdeR−DNA complexes provide additional details of IdeR−DNA interactions that were uncertain in the previous full-length IdeR−DNA complex structure of the identical *mbtA-mbtB* operator sequence at 2.75 Å resolution (*21*) and the DtxR−DNA complex structures at 3.0−3.2 Å resolution (*22*−*24*). Most of the protein−DNA interactions observed in the complex structures involve hydrogen bonds and van der Waals contacts between 2D-IdeR and the DNA phosphate oxygens (Figure 5). However, there are also a number of interactions between the protein and nucleotide bases. Most residues of 2D-IdeR involved in the interactions with the DNA are located in the helix−turn−helix (α2-α3) motif (residues 27−50), which is highly conserved in the iron-dependent repressor protein family (*34*).

The interactions between 2D-IdeR and DNA phosphates cover 23 base pairs. A total of ten residues per subunit are directly engaged in contacts with the phosphate moieties of the DNA (Figure 5). The side chains of four arginine residues (Arg27, Arg29, Arg47, and Arg50) make salt bridges to negatively charged phosphate moieties, while Thr7, Gln36, Ser37, Thr40, and Ser42 use their side chain atoms as hydrogen bond donors for the DNA phosphates. Ala28 and Ser37 make additional contacts with the DNA using their main chain nitrogen atoms. The side chain amide group of Asn2 in all subunits of crystal form I clearly forms hydrogen bonds to OP1 atoms of G15 and C20 from DNA strand E and of C18 and G23 from DNA strand F. In crystal form II, Asn2 is omitted from the model due to weak electron density of the N-terminus.

In both crystal forms, Ser37 and Pro39 interact specifically with thymine bases of the DNA by making similar van der Waals contacts in all subunits (Figure 6 and Table S3) as first described by Chen et al. for DtxR (*24*) and later by Wisedchaisri et al. (*21*) for IdeR. The latter authors define this thymine as T_4 in the $p_1s_2C_3T_4a_5$ recognition fingerprint (Figure 5) based on sequence alignment of known iron boxes. Here, (i) p_1 is a purine (adenine or guanine), (ii) s_2 is a moderately conserved cytosine and can also be guanine if in the central base pair of the iron box, (iii) C_3 is a highly conserved cytosine, (iv) T_4 is a highly conserved thymine, and (v) a_5 is a poorly conserved adenine. Gln43, on the other hand, shows interesting variations in interactions with

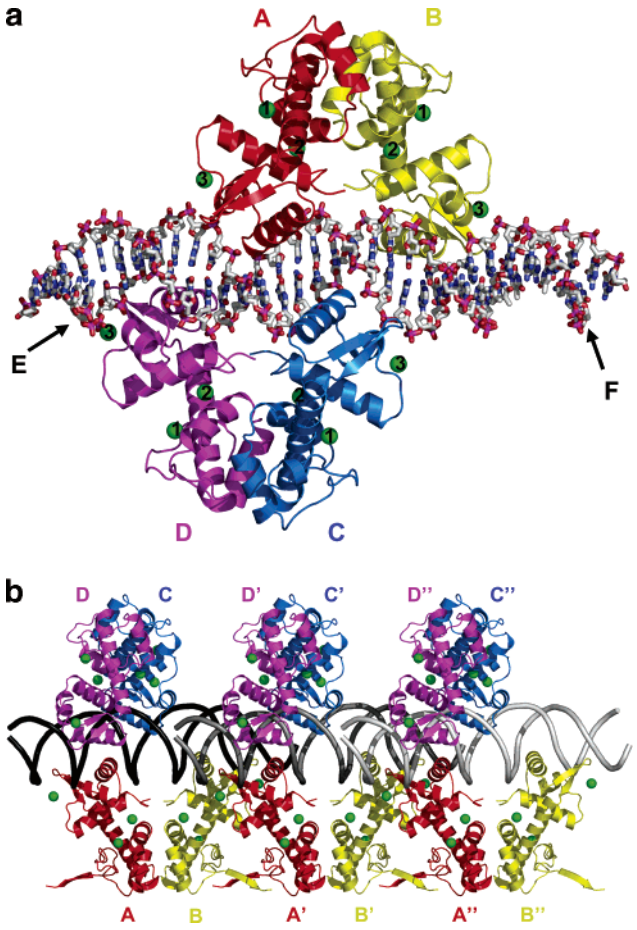

FIGURE 4: Crystal structures of the Ni^{2+}-activated 2D-IdeR−*mbtA-mbtB* operator complex. (a) The 2D-IdeR−DNA complex in crystal form I. The complex contains four 2D-IdeR subunits (A, B, C, and D colored in red, yellow, blue, and magenta, respectively) forming two dimers and one DNA duplex of 33mer oligonucleotides containing the *mbtA-mbtB* operator sequence (stick model labeled strands E and F for *mbtA* and *mbtB*, respectively). Ni^{2+} ions are shown as green spheres. (b) Crystal packing of the 2D-IdeR−DNA complex in crystal form II. The C-terminal tails containing the TEV cleavage sequence of subunits A and B form β-sheets to provide crystal contacts between neighboring molecules on different layers of the semicontinuous DNA helices in the crystal.

nucleotide bases of the DNA. In crystal form I, only the side chain of Gln43 ($O^{\epsilon 1}$ atom) from subunits A and B forms a hydrogen bond to the N4 atom of the cytosine nucleotide base in the s_2 position of the fingerprint (C18F and C20E, respectively) plus additional van der Waals contacts primarily with nearby atoms of the same base (Table S4). The Gln43 side chain of subunits C and D in crystal form I, on the other hand, has a different rotamer that points away from the DNA and does not make contact with any nucleotide bases. This may result from the base type in the s_2 position that is changed to guanine for subunits C and D (G15E and G23F, respectively) in the operator sequence (Table S4). In crystal form II, the Gln43 side chain−DNA interactions of subunits A and B are similar to those found in crystal form I. Additional interactions are observed for the side chain of Gln43 in subunit C of crystal form II making a hydrogen bond to the C16E (N4 atom) nucleotide base. This nucleotide base is not in the s_2 position as those cytosine bases contacted by subunits A and B but is located in the C_3 position. On the basis of the interactions observed in both crystal forms, Gln43 seems to prefer cytosine in the s_2 position as the interaction may be stabilized by a hydrogen bond to the N4 atom of the base. This is the first time where Gln43 of IdeR discriminatingly interacts and makes a hydrogen bond to only cytosine bases. A systematic mutation study of nucleotides in the s_2 position of the fingerprint for IdeR binding affinity will be needed to establish the base specificity for Gln43.

The C-Terminal Tail. In crystal form I, the C-terminal tail of 2D-IdeR (141-ASENLYFQ-148) remaining from the cleavage sequence after proteolysis by TEV protease is not visible in the electron density map for any of the subunits. In crystal form II, however, electron density for the C-terminal ASENLYF tail of subunits A and B forms antiparallel β-sheets with the C-terminal tail of neighboring molecules (Figure 4b). Subunits C and D of crystal form II do not have visible electron density for the C-terminal tails. Crystal contacts of subunits C and D indicate no space for a possibility of β-sheet formation. The β-sheets observed here between subunits A and B are very similar to those found in the structure of 2D-IdeR in the absence of DNA (1.4 Å rms deviation for 14 C^{α} atoms of residues 141−147 calculated for both subunits after the C^{α} atoms of core residues 75−120 were superimposed). The absence of C-terminal tail β-sheet formation in crystal form I could be due to a difference in crystallization condition or the disruption of the contacts by the cyclic decapeptide (C. J. Chou and C. Beeson, unpublished results) present during crystallization which makes it disordered in the electron density map.

Comparison with Full-Length IdeR and the IdeR−DNA Complex. The structures of the 2D-IdeR−DNA complex in both crystal forms are very similar to the 2.75 Å resolution structure of the full-length IdeR−DNA complex (two complexes in the asymmetric unit) determined by Wisedchaisri et al. (*21*) with an average rms deviation of ~0.4 Å for 117 C^{α} atoms of residues 4−120 for a single subunit. The 2D-IdeR−DNA complex structures form a double dimer IdeR−DNA complex arrangement with rms deviations from the full-length complex of 0.6−1.0 Å for 468 C^{α} atoms of residues 4−140 for all four subunits. After the superposition, the operation matrix was then applied to the entire complex in order to calculate an rms deviation of the DNA. The DNA conformations are very similar in the protein-bound region with rms deviations of 0.6−1.1 Å for 46 phosphorus atoms out of 64 backbone phosphates. However, the remaining 18 phosphorus atoms of the DNA outside the protein-bound region are significantly different from those in the full-length complex structure (3.8 and 2.4 Å rms deviation for crystal forms I and II, respectively) despite the identical DNA sequence. The differences in the unbound region of the DNA are possibly due to the flexible nature of the DNA and also to crystal packing interactions with neighboring DNA molecules. In all three structures, Ser37 and Pro39 are the two key residues that make specific base contacts with four signature thymine moieties of the cognate DNA. In both crystal forms only in subunits A and B Gln43 consistently makes hydrogen bonds to N4 atom of cytosine bases (Figure 5 and Table S4) in the s_2 position in the $p_1s_1C_3T_4a_5$ recognition fingerprint. In contrast, in the comparable full-length IdeR−DNA complex (*21*), the Gln43 residues in all subunits make van der Waals contacts to all four different bases in equivalent positions of the DNA.

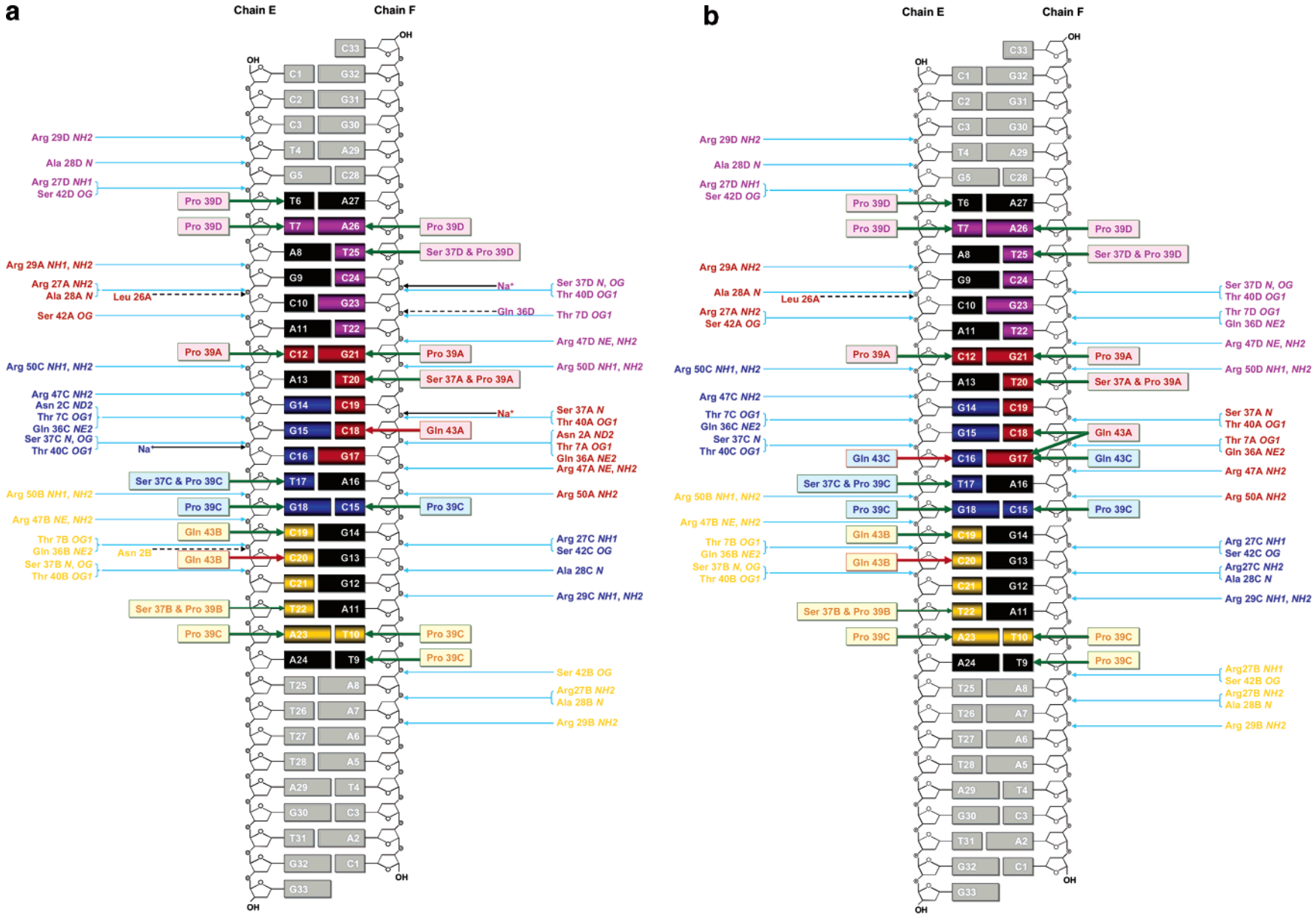

FIGURE 5: Schematic representation of the 2D-IdeR−*mbtA-mbtB* operator contacts. Amino acid residues of IdeR contacting the DNA are colored by subunit, red for A, yellow for B, blue for C, and magenta for D. The 19 base pair iron box of the DNA is highlighted in black with the $p_1s_2C_3T_4a_5$ recognition fingerprint highlighted in the color of the interacting protein subunits. The region outside the iron box is in gray. The base pair G15E-C18F is at the center of the iron box. Protein−DNA backbone hydrogen bonds (<3.3 Å) are shown as cyan arrows. Protein−DNA backbone van der Waals interactions (<3.5 Å) are shown as black broken arrows. Protein−nucleotide base interactions (<3.9 Å) are highlighted in colored boxes and arrows: green for van der Waals interactions of Ser37, Pro39, or Gln43 and red for hydrogen bonds from Gln43. Adapted from Nucplot (*40*) output. (a) 2D-IdeR−DNA interactions in crystal form I. (b) 2D-IdeR−DNA interactions in crystal form II.

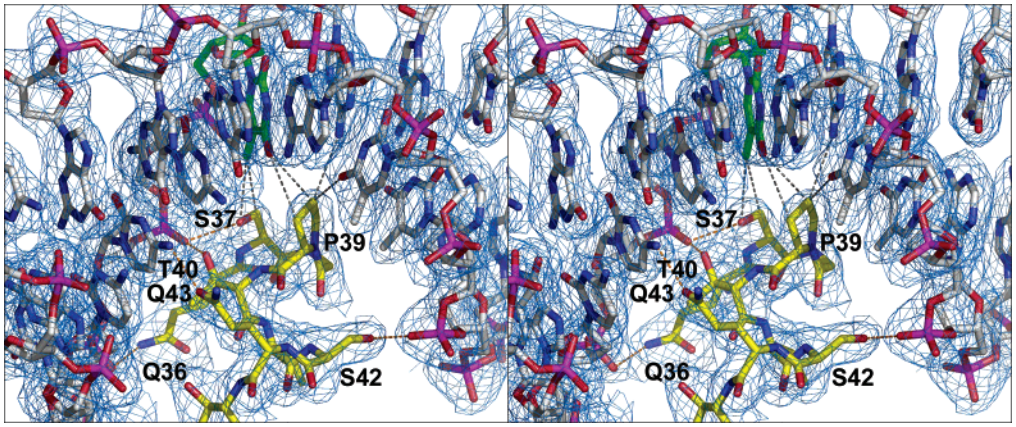

FIGURE 6: IdeR−base specific interactions. Stereoview of the region in subunit B (residues 36−44 shown) of crystal form I where specific interactions between Ser37/Pro39 of IdeR and the signature thymine base of the T22E nucleotide (green) of cognate DNA occur. Ser37 uses its C^{β} and O^{γ} atoms to interact with the methyl group of the thymine while Pro39 makes van der Waals contacts with the thymine O4 atom (plus additional surrounding nucleotide bases) using its C^{β} and C^{γ} atoms. Gln43 uses its $O^{\epsilon 1}$ atom to form a hydrogen bond with the cytosine N4 atom of the C20E nucleotide. The σ_A-weighted $2F_o - F_c$ electron density map is contoured at the 1.0σ level.

It is interesting to note that when only 46 C^{α} atoms of residues 75−120 in the dimerization domain of both subunits in the dimer are used to calculate least-squares superposition, the conformation of the helix−turn−helix motif (residues 27−50) in the Ni^{2+}-activated 2D-IdeR dimer (uncomplexed) (Figure 2a) is closer to that of the dimer in the IdeR−DNA complexes of both full-length (0.6 Å rms deviation for 48 C^{α} atoms) and 2D-IdeR (0.8 Å rms deviation) than to that of the Co^{2+}-activated full-length IdeR dimer (1.0 Å rms deviation) of Feese et al. (*12*). This seems to correlate well with the findings described here and by Chou et al. (*14*) that Ni^{2+} is a better metal activator of IdeR than Co^{2+}. However, it cannot be excluded that the octahedral coordination of metal-binding site 1 in the absence of the SH3-like domain and the oxidation of Cys102 of metal-binding site 2 in the Ni^{2+}-activated 2D-IdeR uncomplexed structure may also play a role in the differences in conformation of the helix−turn−helix motif.

DISCUSSION

The 2D-IdeR protein lacking the SH3-like domain has been characterized. At 1 mg/mL concentration, 2D-IdeR is dimeric in the absence of divalent metal ion, and no intrinsic tryptophan quenching was observed at 2 μM 2D-IdeR. This suggests that 2D-IdeR does not require metal ion for dimerization when the SH3-like domain is not present, and the SH3-like domain may be responsible for dimerization regulation. It was suggested that the function of the SH3-like domain in DtxR is to stabilize the monomer form of the protein in the absence of metal ion (*17*, *18*, *20*), and our results for full-length IdeR (*14*) and 2D-IdeR are consistent with that hypothesis. We proposed (*14*) that the SH3-like domain generally inhibits dimerization of full-length IdeR in the absence of metal ion, making apo-IdeR monomeric in solution at low protein concentration. Previous studies have demonstrated that the SH3-like domain of DtxR can bind to a proline-rich sequence found in the tether region (residues 125−139) with an affinity of 100 μM to 1 mM in one study (*19*) and 740 μM in another study (*20*). (These measurements used a refolded SH3-like domain and a separated proline-rich peptide. Clearly, the effective affinity for intramolecular binding would be higher.) It is possible that in the absence of metal ion, the SH3-like domain normally binds to the tether region and prevents dimerization. This dimerization inhibition is released when divalent metal ion is available. Once metal ion occupies metal-binding site 1, the SH3-like domain moves away from the tether region and binds to metal-binding site 1, allowing IdeR dimerization as observed in crystal structures of fully activated IdeR (*12*, *16*).

Initially, our 2D-IdeR was expressed as a C-terminal His-tagged protein containing an LEH_6 sequence after residue 140. This 2D-IdeR variant showed very little DNA-binding activity (data not shown). Oram et al. (*35*) demonstrated that the 2D-IdeR variant consisting of residues 1−146 with an additional C-terminal LVPR sequence is significantly less active for in vitro DNA binding than its wild-type variant, resulting in very little repressor activity. It is possible that the additional oligopeptide interferes with the functioning of the tether region and can have a profound effect on activity of these 2D-IdeR variants. However, the 2D-IdeR variant described here, after the C-terminal TEV cleavable His_6 tag has been cleaved off, has a very similar activity as wild-type full-length IdeR.

Although metal ions are not required for dimerization, 2D-IdeR binds to the DNA in a metal ion dependent manner. Even at 100-fold excess of 2D-IdeR relative to the *fxbA* operator, there was no evidence of DNA binding in the absence of metal. This observation is consistent with our previous studies showing that the Co^{2+} metal ion affinity for site 1, which mediates dimerization, is distinctly higher than for site 2, which mediates DNA binding (*14*). If the dimer had significant intrinsic affinity for DNA in the absence of metal ion binding to site 2, metal ion mediated dimerization and DNA-binding activation would not have been discriminated. The equilibrium Co^{2+} concentration required for 2D-IdeR binding to the DNA is essentially the same as that for full-length IdeR (*14*) because full-length IdeR forms a dimer at very low Co^{2+} concentrations (K_d for Co^{2+}-dependent IdeR dimerization is less than 0.5 μM) (*14*). The SH3-like domain contributes little, if any, to the second step of activation, which is the alteration of the protein conformation upon binding of Co^{2+} to the metal-binding site 2 and the stabilization of the DNA-binding conformation.

In contrast, the K_d of Ni^{2+} for 2D-IdeR−DNA binding is reduced to 4 μM from 13 μM for full-length IdeR. At 4 μM Ni^{2+} concentration, full-length IdeR is only about 50% dimerized while the 2D-IdeR is already fully dimerized without any added Ni^{2+}. We suggest that the 4 μM K_d measured for 2D-IdeR is the intrinsic affinity of Ni^{2+} for metal-binding site 2, and the 13 μM K_d value obtained for full-length IdeR from the Ni^{2+} titration of DNA binding is a partly averaged affinity for both metal-binding sites 1 and 2.

Our crystal structure of the 2D-IdeR−*mbtA-mbtB* operator complex shows no major conformational difference in the first two domains or the DNA interactions from the structure of the full-length IdeR−DNA complex reported previously (*21*). In addition, 2D-IdeR binds to the *fxbA* operator with similar affinity to that of full-length IdeR in the presence of excess divalent metal ions. This surprising result demonstrates that the SH3-like domain is not critical for DNA binding and may not promote significantly the occurrence of the DNA-binding conformation of IdeR. This is of significant interest since some members of the metal-dependent repressor family, such as *Bacillus subtilis* Mn^{2+}-specific MntR (*36*, *37*) and *Treponema pallidum* TroR (*38*), lack the SH3-like domain. In fact, our 2D-IdeR−DNA structures are the first two-domain variants of the metal-dependent repressor family solved in complex with operator DNA duplexes. The presence of the SH3-like domain in IdeR and DtxR may be required for additional functions such as protein−protein interactions, e.g., with other complexes involved in regulation of gene expression. Since it has been shown that IdeR also functions as a transcription activator of iron-storage genes *bfrA* and *bfrB* containing multiple IdeR-binding sites or iron boxes in their promoter regions (*5*, *6*, *39*), the SH3-like domain may, alternatively or additionally, be involved in interactions between IdeR complexes that bind to the two contiguous iron boxes of the *bfrA* promoter.

On a general level, we observe in two unrelated crystal forms the same antiparallel β-sheet formation between residues remaining from a C-terminal TEV cleavage site (Figures 3 and 4b). This suggests that this sequence might be beneficial in crystallizing other proteins.

ACKNOWLEDGMENT

We gratefully acknowledge the use of the Advanced Photon Source (APS) beamline 19-ID (SBC-CAT) at Argonne National Laboratory and the Advanced Light Source (ALS) beamline 8.2.2 (HHMI) at Lawrence Berkeley National Laboratory and their staffs for technical assistance. Use of the APS and the ALS is supported by the U.S. Department of Energy.

SUPPORTING INFORMATION AVAILABLE

Table S1, equilibrium constants for metal ion activation of 2D-IdeR for binding to the *fxbA* operator; Table S2, metal−ligand distances for all metal-binding sites; Table S3, distance between Ser37/Pro39 and interacting nucleotide bases; Table S4, distance between Gln43 and interacting nucleotide bases; Figure S1, representative dynamic light scattering data. This material is available free of charge via the Internet at http://pubs.acs.org.

REFERENCES

1. Ratledge, C. (2004) Iron, mycobacteria and tuberculosis, *Tuberculosis 84*, 110−130.
2. Frieden, T. R., Sterline, T. R., Munsiff, S. S., Watt, C. J., and Dye, C.(2003) Tuberculosis, *Lancet 362*, 887−899.
3. Dussurget, O., Rodriguez, M., and Smith, I. (1996) An ideR mutant of *Mycobacterium smegmatis* has derepressed siderophore production and an altered oxidative-stress response, *Mol. Microbiol. 22*, 535−544.
4. De Voss, J. J., Rutter, K., Schroeder, B. G., Su, H., Zhu, Y., and Barry, C. E., III (2000) The salicylate-derived mycobactin siderophores of *Mycobacterium tuberculosis* are essential for growth in macrophages, *Proc. Natl. Acad. Sci. U.S.A. 97*, 1252−1257.
5. Gold, B., Rodriquez, G. M., Marras, S. A., Petecost, M., and Smith, I. (2001) The *Mycobacterium tuberculosis* IdeR is a dual functional regulator that controls transcription of genes involved in iron acquisition, iron storage and survival in macrophages, *Mol. Microbiol. 42*, 851−865.
6. Rodriquez, G. M., Voskuil, M. T., Gold, B., Schoolnik, G. K., and Smith, I. (2002) *ideR*, An essential gene in *Mycobacterium tuberculosis*: role of IdeR in iron-dependent gene expression, iron metabolism, and oxidative stress response, *Infect. Immun. 70*, 3371−3381.
7. De Voss, J. J., Rutter, K., Schroeder, B. G., and Barry, C. E., III (1999) Iron acquisition and metabolism by mycobacteria, *J. Bacteriol. 181*, 4443−4451.
8. Crosa, J. H., and Walsh, C. T. (2002) Genetics and assembly line enzymology of siderophore biosynthesis in bacteria, *Microbiol. Mol. Biol. Rev. 66*, 223−249.
9. Quadri, L. E., Sello, J., Keating, T. A., Weinreb, P. H., and Walsh, C. T. (1998) Identification of a *Mycobacterium tuberculosis* gene cluster encoding the biosynthetic enzymes for assembly of the virulence-conferring siderophore mycobactin, *Chem. Biol. 5*, 631−645.
10. Fiss, E. H., Yu, S., and Jacobs, W. R., Jr. (1994) Identification of genes involved in the sequestration of iron in mycobacteria: the ferric exochelin biosynthetic and uptake pathways, *Mol. Microbiol. 14*, 557−569.
11. Dussurget, O., Timm, J., Gomez, M., Gold, B., Yu, S., Sabol, S. Z., Holmes, R. K., Jacobs, W. R. J., and Smith, I. (1999) Transcriptional control of the iron-responsive *fxbA* gene by the mycobacterial regulator IdeR, *J. Bacteriol. 181*, 3402−3408.
12. Feese, M. D., Ingason, B. P., Goranson-Siekierke, J., Holmes, R. K., and Hol, W. G. J. (2001) Crystal structure of the iron-dependent regulator from *Mycobacterium tuberculosis* at 2.0Å resolution reveals the Src homology domain 3-like fold and metal binding function of the third domain, *J. Biol. Chem. 276*, 5959−5966.
13. Qiu, X., Verlinde, C. L., Zhang, S., Schmitt, M. P., Holmes, R. K., and Hol, W. G. J. (1995) Three-dimensional structure of the diphtheria toxin repressor in complex with divalent cation co-repressors, *Structure 3*, 87−100.
14. Chou, C. J., Wisedchaisri, G., Monfeli, R. R., Oram, D. M., Holmes, R. K., Hol, W. G. J., and Beeson, C. (2004) Functional studies of the *Mycobacterium tuberculosis* iron-dependent regulator, *J. Biol. Chem. 279*, 53554−53561.
15. Schmitt, M. P., Predich, M., Doukhan, L., Smith, I., and Holmes, R. K. (1995) Characterization of an iron-dependent regulatory protein (IdeR) of *Mycobacterium tuberculosis* as a functional homolog of the diphtheria toxin repressor (DtxR) from *Corynebacterium diphtheriae*, *Infect. Immun. 11*, 4284−4289.
16. Pohl, E., Holmes, R. K., and Hol, W. G. J. (1999) Crystal structure of the iron-dependent regulator (IdeR) from *Mycobacterium tuberculosis* shows both metal binding sites fully occupied, *J. Mol. Biol. 285*, 1145−1156.
17. Love, J. F., VanderSpek, J. C., and Murphy, J. R. (2003) The src homology 3-like domain of the diphtheria toxin repressor (DtxR) modulates repressor activation through interaction with the ancillary metal ion-binding site, *J. Bacteriol. 185*, 2251−2258.
18. Love, J. F., VanderSpek, J. C., Marin, V., Guerrero, L., Logan, T. M., and Murphy, J. R. (2004) Genetic and biophysical studies of diphtheria toxin repressor (DtxR) and the hyperactive mutant DtxR(E175K) support a multistep model of activation, *Proc. Natl. Acad. Sci. U.S.A. 101*, 2506−2511.
19. Wang, G., Wylie, G. P., Twigg, P. D., Caspar, D. L., Murphy, J. R., and Logan, T. M. (1999) Solution structure and peptide binding studies of the C-terminal src homology 3-like domain of the

diphtheria toxin repressor protein, *Proc. Natl. Acad. Sci. U.S.A. 96*, 6119−6124.
20. Wylie, G. P., Rangachari, V., Bienkiewicz, E. A., Marin, V., Bhattacharya, N., Love, J. F., Murphy, J. R., and Logan, T. M. (2005) Prolylpeptide binding by the prokaryotic SH3-like domain of the diphtheria toxin repressor: a regulatory switch, *Biochemistry 44*, 40−51.
21. Wisedchaisri, G., Holmes, R. K., and Hol, W. G. J. (2004) Crystal structure of an IdeR-DNA complex reveals a conformational change in activated IdeR for base-specific interactions, *J. Mol. Biol. 342*, 1155−1169.
22. White, A., Ding, X., vanderSpek, J. C., Murphy, J. R., and Ringe, D. (1998) Structure of the metal-ion-activated diphtheria toxin repressor/tox operator complex, *Nature 394*, 502−506.
23. Pohl, E., Holmes, R. K., and Hol, W. G. J. (1999) Crystal structure of a cobalt-activated diphtheria toxin repressor-DNA complex reveals a metal-binding SH3-like domain, *J. Mol. Biol. 292*, 653−667.
24. Chen, C. S., White, A., Love, J., Murphy, J. R., and Ringe, D. (2000) Methyl groups of thymine bases are important for nucleic acid recognition by DtxR, *Biochemistry 39*, 10397−10407.
25. Deng, J., Davies, D. R., Wisedchaisri, G., Wu, M., Hol, W. G. J., and Mehlin, C. (2004) An improved protocol for rapid freezing of protein samples for long-term storage, *Acta Crystallogr. D 60*, 203−204.
26. Otwinowski, Z., and Minor, W. (1997) Processing of X-ray diffraction data collected in oscillation mode, *Methods Enzymol. 276*, 307−326.
27. Vagin, A., and Teplyakov, A. (1997) MOLREP: an automated program for molecular replacement, *J. Appl. Crystallogr. 30*, 1022−1025.
28. Murshudov, G. N., Vagin, A. A., and Dodson, E. J. (1997) Refinement of macromolecular structures by the maximum-likelihood method, *Acta Crystallogr. D 53*, 240−255.
29. McRee, D. E. (1999) XtalView/Xfit—A versatile program for manipulating atomic coordinates and electron density, *J. Struct. Biol. 125*, 156−165.
30. Emsley, P., and Cowtan, K. (2004) Coot: model-building tools for molecular graphics, *Acta Crystallogr. D 60*, 2126−2132.
31. Holton, J., and Alber, T. (2004) Automated protein crystal structure determination using ELVES, *Proc. Natl. Acad. Sci. U.S.A. 101*, 1537−1542.
32. Leslie, A. G. W. (1992) Recent changes to the MOSFLM package for processing film and image plate data, *Joint CCP4 + ESF-EAMCB Newsl. Protein Crystallogr. 26.*
33. Evans, P. R. (1993) Data reduction, *Proceedings of CCP4 Study Weekend, 1993, on Data Collection & Processing*, 114−122.
34. Feese, M. D., Hol, W. G. J., Pohl, E., and Holmes, R. K. (2001) Iron-dependent Regulators, in *Handbook of Metalloproteins* (Wieghardt, K., Huber, R., Poulos, T. L., and Messerschmidt, A., Eds.) John Wiley & Sons, West Sussex, U.K.
35. Oram, D. M., Must, L. M., Spinler, J. K., Twiddy, E. M., and Holmes, R. K. (2005) Analysis of truncated variants of the iron dependent transcriptional regulators from *Corynebacterium diphtheriae* and *Mycobacterium tuberculosis*, *FEMS Microbiol. Lett. 243*, 1−8.
36. Que, Q., and Helmann, J. D. (2000) Manganese homeostasis in *Bacillus subtilis* is regulated by MntR, a bifunctional regulator related to the diphtheria toxin repressor family of proteins, *Mol. Microbiol. 35*, 1454−1468.
37. Glasfeld, A., Guedon, E., Helmann, J. D., and Brennan, R. G. (2003) Structure of the manganese-bound manganese transport regulator of *Bacillus subtilis*, *Nat. Struct. Biol. 10*, 652−657.
38. Hardham, J. M., Stamm, L. V., Porcella, S. F., Frye, J. G., Barnes, N. Y., Howell, J. K., Mueller, S. L., Radolf, J. D., Weinstock, G. M., and Norris, S. J. (1997) Identification and transcriptional analysis of a *Treponema pallidum* operon encoding a putative ABC transport system, an iron-activated repressor protein homolog, and a glycolytic pathway enzyme homolog, *Gene 197*, 47−64.
39. Rodriguez, G. M., and Smith, I. (2003) Mechanisms of iron regulation in mycobacteria: role in physiology and virulence, *Mol. Microbiol. 47*, 1485−1494.
40. Luscombe, N. M., Laskowski, R. A., and Thornton, J. M. (1997) NUCPLOT: a program to generate schematic diagrams of protein-nucleic acid interactions, *Nucleic Acids Res. 25*, 4940−4945.

BI0609826